Circular Photogalvanic Effect in Oxide Two-Dimensional Electron Gases

Shuanhu Wang,[1,*] Hui Zhang,[2,*] Jine Zhang,[2,*] Shuqin Li,[1] Dianbing Luo,[1] Jianyuan Wang,[1] Kexin Jin,[1,†] and Jirong Sun[3,4,5,‡]

[1]*Shaanxi Key Laboratory of Condensed Matter Structures and Properties and MOE Key Laboratory of Materials Physics and Chemistry under Extraordinary Conditions, School of Physical Science and Technology, Northwestern Polytechnical University, Xi'an 710072, China*

[2]*School of Integrated Circuit Science and Engineering, Beihang University, Beijing 100191, China*

[3]*Beijing National Laboratory for Condensed Matter Physics and Institute of Physics, Chinese Academy of Sciences, Beijing 100190, China*

[4]*Songshan Lake Materials Laboratory, Dongguan, Guangdong 523808, China*

[5]*Spintronics Institute, University of Jinan, Jinan, Shandong 250022, China*

(Received 10 August 2021; revised 24 November 2021; accepted 28 March 2022; published 4 May 2022)

Two-dimensional electron gases (2DEGs) at the $LaAlO_3/SrTiO_3$ interface have attracted wide interest, and some exotic phenomena are observed, including 2D superconductivity, 2D magnetism, and diverse effects associated with Rashba spin-orbit coupling. Despite the intensive investigations, however, there are still hidden aspects that remain unexplored. For the first time, here we report on the circular photogalvanic effect (CPGE) for the oxide 2DEG. Spin polarized electrons are selectively excited by circular polarized light from the in-gap states of $SrTiO_3$ to 2DEG and are converted into electric current via the mechanism of spin-momentum locking arising from Rashba spin-orbit coupling. Moreover, the CPGE can be effectively modified by the density and distribution of oxygen vacancies. This Letter presents an effective approach to generate and manipulate the spin polarized current, paving the way toward oxide spintronics.

DOI: 10.1103/PhysRevLett.128.187401

The two-dimensional electron gas (2DEG) at the $LaAlO_3/SrTiO_3$ (LAO/STO) heterointerface has been intensively studied since its first discovery in 2004 [1], and diverse phenomena have been observed, such as interfacial superconductivity [2], interfacial ferromagnetism [3], and strong gating effect on interfacial conductance [4–6], etc.

A distinct feature of the 2DEG is spin-momentum locking [7]. Because of the broken spatial inversion symmetry, the 2DEG exhibits a strong Rashba spin-orbit coupling [6,8–11]. Constrained by this mechanism, the electron spin of the 2DEG tends to the direction normal to electron momentum. Via spin-momentum locking, the nonequilibrium spin density induced by, for example, spin pumping can be converted into electric current [12,13] and vice versa [10,14], accomplishing spin-charge interconversion. Spin-momentum locking also leads to additional unusual effects such as nonreciprocal resistive responses to applied dc currents: the resistivity of the 2DEG changes while reversing either the direction of magnetic field or the polarity of applied current [15–17].

Notably, the 2DEG at the LAO/STO interface is composed of Ti $3d$ electrons [18]. Different from the 2DEG, the in-gap states have the character of O $2p$ electrons, emerging accompanying the formation of oxygen vacancies in STO. According to the selection rule of transitions ($\Delta l = \pm 1$, l is the orbital quantum number), it is available to excite electrons from in-gap states to 2DEG. With this in mind, a natural inference is that by transferring the angular momentum of circular photons to in-gap states, electrons with a specific spin direction could be excited from in-gap states to 2DEG. Because of the spin-momentum locking, the interface states will then be asymmetrically depopulated in $\boldsymbol{k}$ space, outputting a spin-polarized electric current in real space [12,13]. This is the so called circular photogalvanic effect (CPGE) [19–21].

Obviously, the CPGE provides a feasible approach to generate and manipulate spin-polarized current [22–24]. However, CPGE has never been explored so far for the 2DEG at the LAO/STO interface though it has been reported for topological insulators [22], Weyl semimetals [25], and other systems [26–30] with relatively simple surface-interface electronic band structures. It is challenging to deal with the 2DEG at the interface of complex perovskite oxides.

In this Letter, we report on the observation of strong CPGE for complex oxide 2DEG, created by exciting in-gap states to 2DEG with circularly polarized light. We identified the distinct feature of CPGE from the complex oscillation of the photovoltaic signal with the degree of circular polarization of the incident light. We also found a strong dependence of the CPGE on the incident direction of the light, the density of oxygen vacancies or in-gap states, and electric gate.

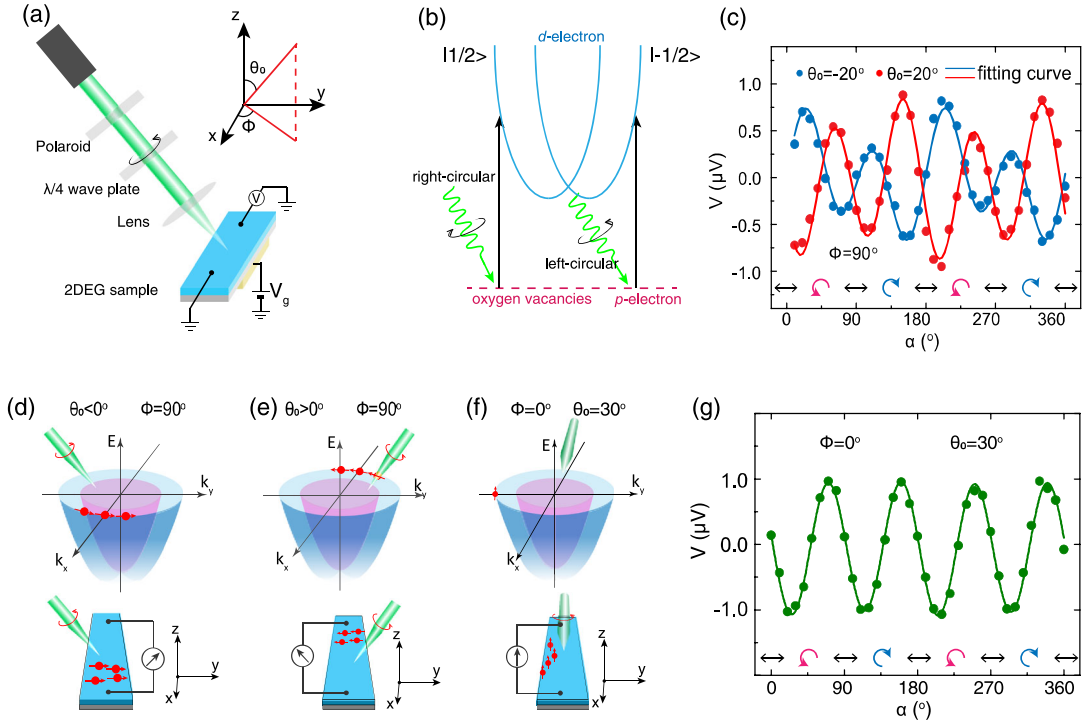

FIG. 1. (a) Sketches for the CPGE measurements. Circularly polarized incident light is introduced into the 2DEG sample with two electrodes arranged along the x axis. The polar angle θ_0 and azimuth angle ϕ of the incident light are defined in the figure. (b) A schematic diagram for the mechanism of CPGE. The Rashba effect occurs at the LAO/STO interfaces where the broken spatial symmetry removes $\boldsymbol{k}$-space spin degeneracy of the $3d$ band structure. The energy level of oxygen vacancies locates in the band gap of STO. The circularly polarized light will selectively excite electrons in defect levels to the specific conduction band (black arrow), generating a transverse spin polarized electric current along the x axis in real space. (c),(g) Photovoltage as a function of laser polarization for (111)-LAO/STO 2DEG with a carrier density of 4.9×10^{14} cm^{-2}, with differently directed incident light. Dots are experimental data, and lines are data fitting to Eq. (1). The power of the light is 27 mW. All measurements were conducted at room temperature. (d)–(f) illustrate the distribution of photogenerated electrons, which are excited by left-circular light from different directions, in reciprocal (upper panel) and real (bottom panel) spaces.

Oxide 2DEGs at the LAO/STO interfaces were fabricated by pulsed laser deposition following the procedure described in Supplemental Material [31]. To introduce oxygen vacancies, notably, the samples were growth in appropriately high vacuum atmosphere without *in situ* post annealing in oxygen atmosphere. Therefore, the interface is not conventional. In the present experiment, 532 nm light passed through successively a polaroid and a $\lambda/4$ waveplate, and then focused on sample surface by a lens, with a spot size of $\sim$100 μm in diameter [see Fig. 1(a)]. The polar angle is θ_0 and the azimuth angle is ϕ for the incident light. The degree of the circular polarization of the incident light was tuned by rotating the $\lambda/4$ wave plate by an angle of α. The output light will be left (right) circularly polarized when α equals to 45° or 225° (135° or 315°) and linearly polarized when α is an integral multiple of 90°. Light illumination will generate a photoelectric output if the light is circularly polarized as explained later. Photovoltage was recorded by a nanovoltmeter (Keithley 2182). Here, we presented photovoltage instead of photocurrent because of its high signal-to-noise ratio [31]. The separation of the electrodes was 0.8 mm, connected to the interface of the 2DEG.

Since the photon energy is much smaller than the band gap of STO ($\sim$2.3 eV versus $\sim$3.2 eV), mainly the electrons of in-gap states, which own the character of oxygen vacancy, are excited to 2DEG [see Fig. 1(b)]. Notably, the circular light will selectively excite the in-gap states with a specific spin direction, resulting in spin polarized 2DEG. This spin polarization in turn leads to a variation in electron momentum along the direction perpendicular to spin polarization, yielding an electric current in the case of short circuit or an electric voltage in the case of open circuit. As well documented [7,26], there is an orthogonal locking between electron spin and electron momentum due to the Rashba spin-orbit coupling at the LAO/STO interface, and any changes in spin polarization will have responses in electron momentum (a more detailed explanation on the physical mechanism of the photoelectric effect can be found in Sec. 3 of Supplemental Material [31]).

Figure 1(c) shows the photovoltage as a function of α for the (111)-oriented 2DEG, collected with the incident direction of $\theta_0 = -20°$ or 20° (light power = 27 mW). There is a background voltage V_0 that linearly grows with the distance of the light spot from the middle point of two

electrodes ($x = 0$), as shown in Fig. S4 of Supplemental Material [31]. To get a high signal-to-noise ratio, all data presented here are collected by locating light spot at the position of $x = 0$ and setting ϕ to 90° (unless otherwise indicated).

Two features can be identified from the V-α curves. First, the experimental data display a regular oscillation with two different amplitudes, indicating the occurrence of two processes. Second, switching the incident angle of polarized light from θ_0 to $-\theta_0$, the V-α curve reverses. To identify the contribution of the CPGE, we perform a further analysis of the V-α curves. As reported, the photovoltage will show a complex oscillation against the rotation angle of the $\lambda/4$ wave plate when the incident light is oblique ($\theta_0 \neq 0$) [22,23,29,30],

$$V = V_{\mathrm{CPGE}} \sin 2\alpha + L_1 \sin 4\alpha + L_2 \cos 4\alpha + V_0, \quad (1)$$

where V_0 is a background voltage resulting from the lateral photogalvanic effect and the effect of thermal gradients produced by laser heating, V_{CPGE} parametrizes the CPGE which is helicity dependent, and L_1 and L_2 stem from the linear photogalvanic effect (LPGE) or photon drag effect [22,29] which is independent of light helicity. V_{CPGE} changes sign if the polarization is switched from left to right circularity. CPGE vanishes for linearly polarized light, corresponding to the α value of an integral multiple of 90°.

By fitting the experimental data to Eq. (1), we obtain the V_{CPGE} of 0.27 μV and -0.22 μV, corresponding to the θ_0 of 20° and −20°. The corresponding L_1 and L_2 are 0.46 μV and -0.2 μV for $\theta_0 = -20°$ and -0.61 μV and 0.17 μV for $\theta_0 = 20°$. These results confirm the appearance of CPGE in 2DEG. In the following analysis, we will focus on V_{CPGE}. Notably, the magnitudes of V_{CPGE} are close to each other whereas the signs of V_{CPGE} are opposite when reversing the sign of θ_0, i.e., altering the sign of θ_0 changes the sign of V_{CPGE}. As shown in Figs. 1(d) and 1(e), when a left-circular light, for example, is obliquely incident in the $\theta_0 = -20°$ and 20°, the projection of the angular momentum of the light in the x-y plane is opposite to each other. Therefore, the transferred angular momentum to the excited electrons is reversed. This means that circular light incident in opposite polar angle will excite electrons with opposite spin polarization. Because of the orthogonal locking between electron spin direction and electron momentum, oppositely incident light will generate an opposite flow of electrons and thus opposite current. The dependence of V_{CPGE} on light intensity is also investigated, and $|V_{\mathrm{CPGE}}|$ exhibits a linear growth with light power [31].

When incident light is in the z-x plane ($\phi = 0$) V_{CPGE} becomes invisible and only LPGE is detectable even for nonzero θ_0 [Fig. 1(g)]. For this configuration, the light is incident in the x-z plane, and the projection of the angular momentum of light is zero along the y direction. Therefore, it will only excite the electron with a spin polarization along the $\boldsymbol{k}_x$ direction or a momentum along the $\boldsymbol{k}_y$ direction [see Fig. 1(f)]. In this case, the electron will move in the y direction in real space. This direction is normal to the electrode direction, and, as a consequence, no CPGE signal will be detected.

The CPGE can be described by the following phenomenological expression [19,26,27]:

$$V_{\mathrm{CPGE}} = \gamma_{\lambda\mu} i(E \times E^*)_\mu, \quad (2)$$

$$i(E \times E^*)_\mu = \hat{e}_\mu E_0^2 P_{\mathrm{circ}}, \quad (3)$$

where $\gamma_{\lambda\mu}$ is the pseudotensor which is related to the symmetry of the material. The E and P_{circ} stand for the complex amplitude of the electric field of the electromagnetic wave and the degree of the circular polarization, respectively. E_0^2 is proportional to the radiation power. $\hat{e}_\mu$ describes the unit vector pointing to the direction of light propagation. For the configuration of our measurement, the λ and μ represent the x and y direction, respectively, and the $\hat{e}_y$ is given by

$$\hat{e}_y = t_p t_s \sin\theta. \quad (4)$$

According to Fresnel's formula,

$$t_p t_s = \frac{4\cos^2\theta_0}{(\cos\theta_0 + \sqrt{\varepsilon^* - \sin^2\theta_0})(\varepsilon^* \cos\theta_0 + \sqrt{\varepsilon^* - \sin^2\theta_0})}, \quad (5)$$

where the t_p, t_s stand for the transmission coefficients for linear p and s polarizations. Since the light was obliquely incident on the sample, the areas of the light spot would be $S/\cos\theta_0$, where the S is the cross-sectional area of light. The refraction angle θ is defined by

$$\sin\theta = \frac{\sin\theta_0}{\sqrt{\varepsilon^*}}, \quad (6)$$

where ε^* is dielectric constant. Using Eqs. (2)–(6), V_{CPGE} can be related to θ_0 by

$$V_{\mathrm{CPGE}} \propto \frac{4P_{\mathrm{circ}}\cos\theta_0 \sin\theta_0}{(\cos\theta_0 + \sqrt{\varepsilon^* - \sin^2\theta_0})(\varepsilon^* \cos\theta_0 + \sqrt{\varepsilon^* - \sin^2\theta_0})}. \quad (7)$$

Equation (7) suggests a close relation between V_{CPGE} and θ_0. To further confirm the occurrence of CPGE, the dependence of V_{CPGE} on incident angle θ_0 is investigated. As shown in Fig. 2, V_{CPGE} is zero when $\theta_o = 0$ and monotonically increases with θ_0. Notably, the growth rate of V_{CPGE} against θ_0 slightly slows down when θ_0 is large, resulting in a curved $V_{\mathrm{CPGE}} - \theta_0$ curve. This is a general feature, observed in three differently oriented 2DEGs.

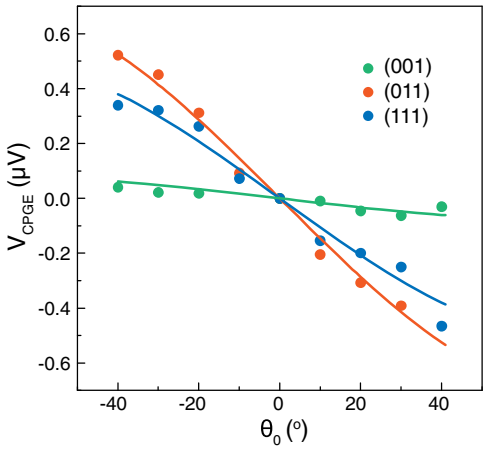

FIG. 2. V_{CPGE} as a function of incident angle θ_0. V_{CPGE} is different oriented samples. Solid symbols are experimental data and solid curves are results of curve fitting based Eq. (7).

Adopting suitable fitting parameters, the $V_{CPGE} - \theta_0$ curves are satisfactorily reproduced by Eq. (7), including detailed features. This result gives us further evidence that V_{CPGE} indeed stems from CPGE. Here, the V_{CPGE} is different for (001), (011), and (111) 2DEGs, which could be related to the different densities of in-gap states and different symmetry of the interface [31].

As suggested by the above experiments, spin polarized electrons are excited from the in-gap states in STO, with the character of oxygen vacancy. Notably, for the conventional interface where the content of oxygen vacancies is minimized, the CPGE may be weak even absent. Considering the fact that the in-gap states are mainly composed of the oxygen vacancies with trapped electrons, a natural inference is that the CPGE should be a function of the content of oxygen vacancies. Indeed, we observed a close relation between CPGE and the content of oxygen vacancies. A series of (111)-2DEGs were fabricated under the oxygen pressures from 5 to 0.1 mPa, without postannealing in the oxygen atmosphere. In this case, the mobile electrons of 2DEG come mainly from oxygen vacancies which act as electron donors. Further experiment gives the corresponding carrier densities (n_s) ranging from $\sim 1 \times 10^{14}$ cm^{-2} to $\sim 6.2 \times 10^{15}$ cm^{-2}. The procedure for the determination of carrier density (n_s) and mobility for these samples is presented in Supplemental Material [31]. As oxygen pressure decreases, the content of oxygen vacancies increases accordingly, providing more mobile electrons to 2DEG. As expected, the CPGE displays a remarkable enhancement with increasing n_s. As shown in Fig. 3, V_{CPGE} is $0.2 \sim 0.3$ μV when n_s is around 10^{14} cm^{-2} and suddenly jumps to ~ 1 μV when n_s exceeds $\sim 10^{15}$ cm^{-2}. It is a natural expectation that a high density of the in-gap states will result in a high probability for the in-gap states to be excited. Figure 3(b) shows a comparison of the CPGE for two 2DEGs with obviously different densities of charge carriers or oxygen vacancies.

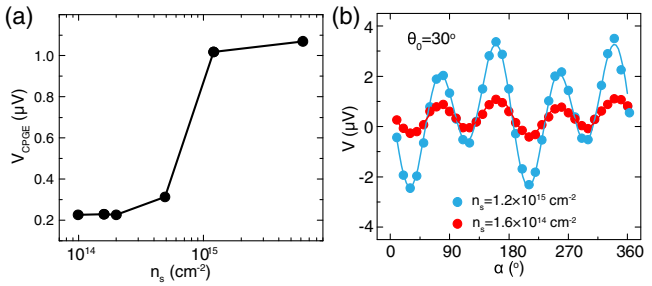

FIG. 3. (a) CPGE as a function of carrier densities for (111)-LAO/STO. The obvious increase in V_{CPGE} takes place when n_s exceeds 10^{15} cm^{-2}. (b) Photovoltages as a function of α, collected for two samples with different carrier densities. Light power is 27 mW.

The above results demonstrate the strong effect of oxygen vacancies on CPGE. In fact, in addition to density, the distribution of oxygen vacancies in STO can also be tuned. As reported, the oxygen vacancies in STO tend to drift along the electrical field. Particularly, they will exhibit an accelerated migration rate after being excited by photoillumination [35]. We choose the (011) and (111) LAO/STO as examples because they have the larger V_{CPGE} [Fig. 2(a)]. To collect the photovoltage with a high signal-to-noise ratio, the sample was placed in a shielding box, and the sample surface and the shielding box were connected to ground. The schematic of the wire connection is illustrated in the inset of Fig. 4(a). Measurements were carried out after the application of the gating field for 10 min to make sure the sample stays in a stable state [36]. Figure 4(a) presents the CPGE voltage measured as a function of perpendicular electric field. In the depletion regime ($V_g < 0$), oxygen vacancies will drift away from the interface. In this case, the photoexcited electron must travel a long distance to reach the 2DEG layer. Consequently, the recombination probability is enhanced and the CPGE is weakened. It is experimentally shown that V_{CPGE} is ~ 0.33 μV under the gate field of -20 V for (011) LAO/STO. In the accumulation regime ($V_g > 0$), oxygen vacancies will migrate toward the interface. As a result, the separation between excited electrons and 2DEG is short and the recombination probability is decreased. Accordingly, the CPGE is enhanced. According to Fig. 4(a), V_{CPGE} is 1.1 μV under a gate voltage of 40 V for (011) LAO/STO. Figure 4(b) shows the V_{CPGE}-α relations collected under the gate voltage of -20 V (blue) and 40 V (red), respectively. The difference caused by different gate voltages can be clearly seen. Notably, the leak current induced by the light-assisted electrostatic gating is negligible [31].

Furthermore, the CPGE of the (001) and (111) LAO/KTO interface is also investigated. The magnitude of CPGE at LAO/KTO is close to that of LAO/STO [31].

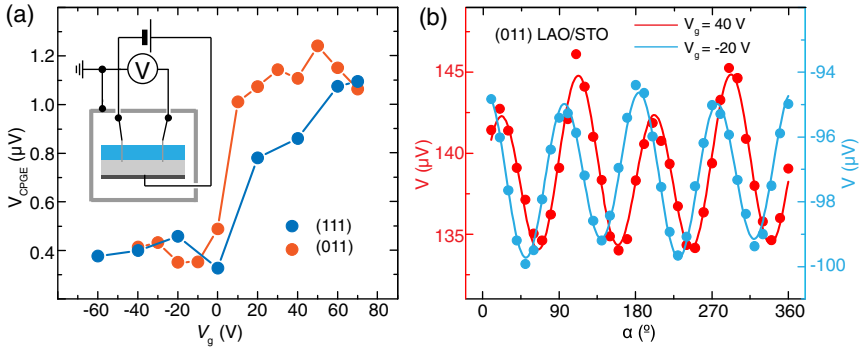

FIG. 4. (a) V_{CPGE} as a function of gate voltage. Inset: a schematic diagram for experiment setup. (b) Photovoltages as functions of α, collected under the gate voltages of −20 and 40 V, respectively. Solid symbols are experimental results and solid curves are results of curve fitting based on Eq. (1).

In summary, the CPGE has been observed in oxide 2DEG, and its relation with the degree of circular polarization of incident light, oxygen vacancies, and the electric gate has been established. A complex oscillation of photovoltage with the degree of circular polarization of the incident light is observed, and the component associated with CPGE is identified. Further analysis indicates a selective excitation of the in-gap states by circular polarized light. The excited electrons are converted into electric current by spin-momentum locking of the 2DEG. Tuning in-gap states (or oxygen vacancies) tunes the CPGE. This Letter uncovers a hidden aspect of the 2DEG, deepening our understanding of oxide 2DEG.

Project supported by the Natural Science Foundation of Shaanxi Province, China (Grant No. 2020JM-088), the Science Center of the National Science Foundation of China (No. 52088101), the National Natural Science Foundation of China (Grants No. 51572222, No. 12004022, No. 11934016, No. 51701158, No. 52130405, and No. 51872241), the National Key R&D Program of China (No. 2018YFA0305704, No. 2021YFA1400300, and No. 2017YFA0303601), the Strategic Priority Research Program (B) (No. XDB33030200), the key research program (No. ZDRW-CN-2021-3 and No. QYZDY-SSW-SLH020) of the Chinese Academy of Sciences. J. R. S. is thankful for the support of the Project for Innovative Research Team of National Natural Science Foundation of China (No. 111921004). We would like to thank the Analytical & Testing Center of Northwestern Polytechnical University for PPMS characterization.

*These authors contributed equally to this work.
†Corresponding author.
jinkx@nwpu.edu.cn
‡Corresponding author.
jrsun@iphy.ac.cn

[1] A. Ohtomo and H. Y. Hwang, Nature (London) **427**, 423 (2004).
[2] N. Reyren, S. Thiel, A. D. Caviglia, L. F. Kourkoutis, G. Hammerl, C. Richter, C. W. Schneider, T. Kopp, A. S. Ruetschi, D. Jaccard, M. Gabay, D. A. Muller, J. M. Triscone, and J. Mannhart, Science **317**, 1196 (2007).
[3] A. Brinkman, M. Huijben, M. Van Zalk, J. Huijben, U. Zeitler, J. C. Maan, W. G. Van der Wiel, G. Rijnders, D. H. A. Blank, and H. Hilgenkamp, Nat. Mater. **6**, 493 (2007).
[4] A. D. Caviglia, S. Gariglio, N. Reyren, D. Jaccard, T. Schneider, M. Gabay, S. Thiel, G. Hammerl, J. Mannhart, and J. M. Triscone, Nature (London) **456**, 624 (2008).
[5] S. Thiel, G. Hammerl, A. Schmehl, C. W. Schneider, and J. Mannhart, Science **313**, 1942 (2006).
[6] M. Ben Shalom, M. Sachs, D. Rakhmilevitch, A. Palevski, and Y. Dagan, Phys. Rev. Lett. **104**, 126802 (2010).
[7] Y. A. Bychkov and E. I Rashba, JETP Lett. **39**, 78 (1984).
[8] A. D. Caviglia, M. Gabay, S. Gariglio, N. Reyren, C. Cancellieri, and J. M. Triscone, Phys. Rev. Lett. **104**, 126803 (2010).
[9] Z. Zhong, A. Tóth, and K. Held, Phys. Rev. B **87**, 161102 (R) (2013).
[10] H. Yang, B. Zhang, X. Zhang, X. Yan, W. Cai, Y. Zhao, J. Sun, K. L. Wang, D. Zhu, and W. Zhao, Phys. Rev. Applied **12**, 034004 (2019).
[11] H. R. Zhang, Y. Ma, H. Zhang, X. B. Chen, S. H. Wang, G. Li, Y. Yun, X. Yan, Y. S. Chen, F. X. Hu, J. W. Cai, B. G. Shen, W. Han, and J. R. Sun, Nano Lett. **19**, 1605 (2019).
[12] E. Lesne, Y. Fu, S. Oyarzun, J. C. Rojas-Sanchez, D. C. Vaz, H. Naganuma, G. Sicoli, J. P. Attane, M. Jamet, E. Jacquet, J. M. George, A. Barthelemy, H. Jaffres, A. Fert, M. Bibes, and L. Vila, Nat. Mater. **19**, 1261 (2019).
[13] Q. Song, H. Zhang, T. Su, W. Yuan, Y. Chen, W. Xing, J. Shi, J. Sun, and W. Han, Sci. Adv. **3**, e1602312 (2017).
[14] Y. Wang, R. Ramaswamy, M. Motapothula, K. Narayanapillai, D. Zhu, J. Yu, T. Venkatesan, and H. Yang, Nano Lett. **17**, 7659 (2017).
[15] D. Choe, M.-J. Jin, S.-I. Kim, H.-J. Choi, J. Jo, I. Oh, J. Park, H. Jin, H. C. Koo, B.-C. Min, S. Hong, H.-W. Lee, S.-H. Baek, and J.-W. Yoo, Nat. Commun. **10**, 4510 (2019).
[16] T. Guillet, C. Zucchetti, Q. Barbedienne, A. Marty, G. Isella, L. Cagnon, C. Vergnaud, H. Jaffrès, N. Reyren, J. M. George, A. Fert, and M. Jamet, Phys. Rev. Lett. **124**, 027201 (2020).

[17] J. Zhang, H. Zhang, X. Chen, J. Zhang, S. Qi, F. Han, Y. Chen, W. Zhao, F. Hu, B. Shen, and J. Sun, Phys. Rev. B **104**, 045114 (2021).
[18] P. D. C. King, S. M. Walker, A. Tamai, A. de la Torre, T. Eknapakul, P. Buaphet, S. K. Mo, W. Meevasana, M. S. Bahramy, and F. Baumberger, Nat. Commun. **5**, 3414 (2014).
[19] V. M. Asnin, A. A. Bakun, A. M. Danishevskii, E. L. Ivchenko, G. E. Pikus, and A. A. Rogachev, Solid State Commun. **30**, 565 (1979).
[20] V. I. Belinicher, Phys. Lett. A **66**, 213 (1978).
[21] E. L. Ivchenko and G. E. Pikus, JETP Lett. **27**, 604 (1978).
[22] J. W. McIver, D. Hsieh, H. Steinberg, P. Jarillo-Herrero, and N. Gedik, Nat. Nanotechnol. **7**, 96 (2012).
[23] J. L. Yu, X. L. Zeng, L. G. Zhang, K. He, S. Y. Cheng, Y. F. Lai, W. Huang, Y. H. Chen, C. M. Yin, and Q. K. Xue, Nano Lett. **17**, 7878 (2017).
[24] Y. Yan, Z.-M. Liao, X. Ke, G. Van Tendeloo, Q. Wang, D. Sun, W. Yao, S. Zhou, L. Zhang, H.-C. Wu, and D.-P. Yu, Nano Lett. **14**, 4389 (2014).
[25] F. De Juan, A. G. Grushin, T. Morimoto, and J. E. Moore, Nat. Commun. **8**, 15995 (2017).
[26] S. D. Ganichev and W. Prettl, J. Phys. Condens. Matter **15**, R935 (2003).
[27] S. D. Ganichev, H. Ketterl, W. Prettl, E. L. Ivchenko, and L. E. Vorobjev, Appl. Phys. Lett. **77**, 3146 (2000).
[28] X. W. He, B. Shen, Y. H. Chen, Q. Zhang, K. Han, C. M. Yin, N. Tang, F. J. Xu, C. G. Tang, Z. J. Yang, Z. X. Qin, G. Y. Zhang, and Z. G. Wang, Phys. Rev. Lett. **101**, 147402 (2008).
[29] S. Hubmann, G. V. Budkin, M. Otteneder, D. But, D. Sacré, I. Yahniuk, K. Diendorfer, V. V. Bel'kov, D. A. Kozlov, N. N. Mikhailov, S. A. Dvoretsky, V. S. Varavin, V. G. Remesnik, S. A. Tarasenko, W. Knap, and S. D. Ganichev, Phys. Rev. Mater. **4**, 043607 (2020).
[30] X. J. Liu, A. Chanana, U. Huynh, F. Xue, P. Haney, S. Blair, X. M. Jiang, and Z. V. Vardeny, Nat. Commun. **11**, 323 (2020).
[31] See Supplemental Material at http://link.aps.org/supplemental/10.1103/PhysRevLett.128.187401 for the details of the sample fabrication, carrier concentration and mobility, CPGE as a function of the light spot and light power, the effect of the leak current on CPGE, and CPGE in KTaO3/SrTiO3, which includes Refs. [32–34].
[32] Z. H. Yang, Y. S. Chen, H. R. Zhang, H. L. Huang, S. F. Wang, S. H. Wang, B. G. Shen, and J. R. Sun, Appl. Phys. Lett. **111**, 231602 (2017).
[33] H. Yan, Z. Zhang, M. Li, S. Wang, L. Ren, and K. Jin, J. Phys. Condens. Matter **32**, 135002 (2020).
[34] Y. Y. Tian, S. H. Wang, H. Zhang, H. Li, S. Q. Li, M. K. Butt, Y. Zhao, J. Y. Wang, and K. X. Jin, J. Phys. D **53**, 225102 (2020).
[35] Y. Lei, Y. Li, Y. Z. Chen, Y. W. Xie, Y. S. Chen, S. H. Wang, J. Wang, B. G. Shen, N. Pryds, H. Y. Hwang, and J. R. Sun, Nat. Commun. **5**, 5554 (2014).
[36] H. Zhang, X. Yan, X. J. Zhang, S. Wang, C. M. Xiong, H. R. Zhang, S. J. Qi, J. N. Zhang, F. R. Han, N. Wu, B. G. Liu, Y. S. Chen, B. G. Shen, and J. R. Sun, ACS Nano **13**, 609 (2019).